Readily releasable pool of synaptic vesicles measured at single synaptic contacts

Federico F. Trigo[a], Takeshi Sakaba[b,c], David Ogden[a], and Alain Marty[a,1]

[a]Laboratoire de Physiologie Cérébrale, Centre National de la Recherche Scientifique and Université Paris Descartes, 75006 Paris, France; [b]Graduate School of Brain Science, Doshisha University, Kizugawa-shi, 6190225 Kyoto, Japan; and [c]Max Planck Institute for Biophysical Chemistry, 37077 Gottingen, Germany

Edited by Erwin Neher, Max Planck Institute of Biophysical Chemistry, Gottingen, Germany, and approved September 18, 2012 (received for review June 8, 2012)

To distinguish between different models of vesicular release in brain synapses, it is necessary to know the number of vesicles of transmitter that can be released immediately at individual synapses by a high-calcium stimulus, the readily releasable pool (RRP). We used direct stimulation by calcium uncaging at identified, single-site inhibitory synapses to investigate the statistics of vesicular release and the size of the RRP. Vesicular release, detected as quantal responses in the postsynaptic neuron, showed an unexpected stochastic variation in the number of quanta from stimulus to stimulus at high intracellular calcium, with a mean of 1.9 per stimulus and a maximum of three or four. The results provide direct measurement of the RRP at single synaptic sites. They are consistent with models in which release proceeds from a small number of vesicle docking sites with an average occupancy around 0.7.

release site | exocytosis | interneurons | cerebellum

Detailed characterization of elementary synaptic signals in the mammalian nervous system is a prerequisite to understanding the mechanisms of synaptic transmission, from both physiological and molecular perspectives. A major impetus in this direction was given by the description of miniature postsynaptic potentials in the frog neuromuscular junction and by the demonstration of their participation in evoked synaptic responses (1, 2), leading to the development and gradual acceptance of the quantal hypothesis of transmitter release.

Unlike the neuromuscular junction, mammalian central synapses have clearly defined release sites that differ widely in morphological, molecular, and functional properties (3–5). How these may influence signaling remains unclear because the small size of the presynaptic compartment of most central synapses has hindered electrophysiological and optical studies of quantal release at single functional sites. In cultured neurons, styryl dye fluorescence can deliver quantal measurements in single varicosities (6), but optical methods are difficult to adapt to integrated preparations, such as brain slices. In general, the development of optical recording to study individual exocytosis events in single synapses is challenging (7). In particular, there has been no direct measurement of a key biophysical parameter: the number of quanta that can be immediately released by strong stimulation, the "readily releasable pool" (RRP) of synaptic vesicles. Previously, indirect methods have given widely different estimates for the RRP at single release sites, generating uncertainties on the structural and functional significance of the RRP (8). A reliable estimate is important because the RRP is central in distinguishing between functional models of synaptic transmission (9) and also in models of short-term synaptic plasticity (10).

Although optical methods have been used successfully to monitor synaptic activity in the brain (11–13), electrophysiological methods remain the most sensitive assay of quantal signals. In this work, we combine electrophysiological (whole-cell patch-clamp recording) and optical methods (uncaging of Ca^{2+} with a small-diameter laser spot) to study single synaptic contacts of GABAergic synapses in the cerebellum. Ca^{2+} uncaging has been used successfully to study synaptic transmission in large glutamatergic synapses (14–16), in large GABAergic synapses (17), and in autapses in culture (18). However, to the best of our knowledge, it has never been used to study synaptic contacts with a single release site. Here, using cerebellar interneurons as a model, we provide direct measurements of the RRP and related biophysical parameters of transmission in small inhibitory cerebellar synapses.

Results

Ca^{2+} Uncaging at Individual Synaptic Contacts. To study quantal release and the RRP directly, we identified individual synaptic connections and measured quantal events evoked postsynaptically by presynaptic calcium uncaging with localized laser light. Inhibitory synapses among cerebellar molecular layer interneurons (MLIs; stellate and basket cells) were used because they make only a few synaptic contacts on their postsynaptic partner and because each connection exhibits a large quantal size, on the order of 200 pA at resting potential under symmetrical Cl^- conditions (3, 19, 20). Our strategy was to establish a recording from a synaptically connected pair of MLIs and to find the synaptic contacts between the two neurons. We then produced a rapid and uniform increase of intracellular Ca^{2+} by photolysis of the caged-calcium chelator 1-(2-nitro-4,5-dimethoxyphenyl)-N,N,N′,N′-tetrakis[(oxycarbonyl)methyl]-1,2-ethanediamine (DM-nitrophen) (21) with a laser spot similar in size (diameter of 1–5 μm) to the presynaptic terminal (22) (Fig. 1*A*). The presynaptic cell was recorded with an intracellular solution containing Alexa 594 to aid in identification (red in Fig. 1 *A* and *B*), a high millimolar concentration of DM-nitrophen loaded with Ca^{2+} and, in some experiments, with the calcium indicator Oregon Green BAPTA-5N (OGB-5N). The postsynaptic cell was recorded with a KCl-based intracellular solution containing Alexa 488 to distinguish it from the presynaptic cell (green in Fig. 1 *A* and *B*). The presence of synaptic connections was tested by inducing unclamped action potentials (APs) in the axon of the presynaptic cell (Fig. 1*C*, *Left*).

After establishing the presence of a synaptic connection, we searched for the contacts by carefully following the presynaptic axon while alternating between blue (470 nm) and amber (572 nm) fluorescence excitation to distinguish between presynaptic and postsynaptic cells (Fig. S1*A* and Movie S1). In juvenile MLIs, axonal and dendritic compartments are readily distinguished, allowing the identification of potential synaptic contacts. Fig. 1*C* compares the postsynaptic currents (PSCs) induced by the electrical stimulation of the presynaptic cell (Fig. 1*C*, *Left*) or the laser spot (Fig. 1*C*, *Right*) focused to the site of contact, shown with the arrowheads in Fig. 1*B*. The spike-induced PSC is monophasic, as

Author contributions: F.F.T., T.S., D.O., and A.M. designed research; D.O. designed and built the equipment; F.F.T. performed research; F.F.T., T.S., D.O., and A.M. analyzed data; and F.F.T., D.O., and A.M. wrote the paper.

The authors declare no conflict of interest.

This article is a PNAS Direct Submission.

[1]To whom correspondence should be addressed. E-mail: alain.marty@parisdescartes.fr.

This article contains supporting information online at www.pnas.org/lookup/suppl/doi:10.1073/pnas.1209798109/-/DCSupplemental.

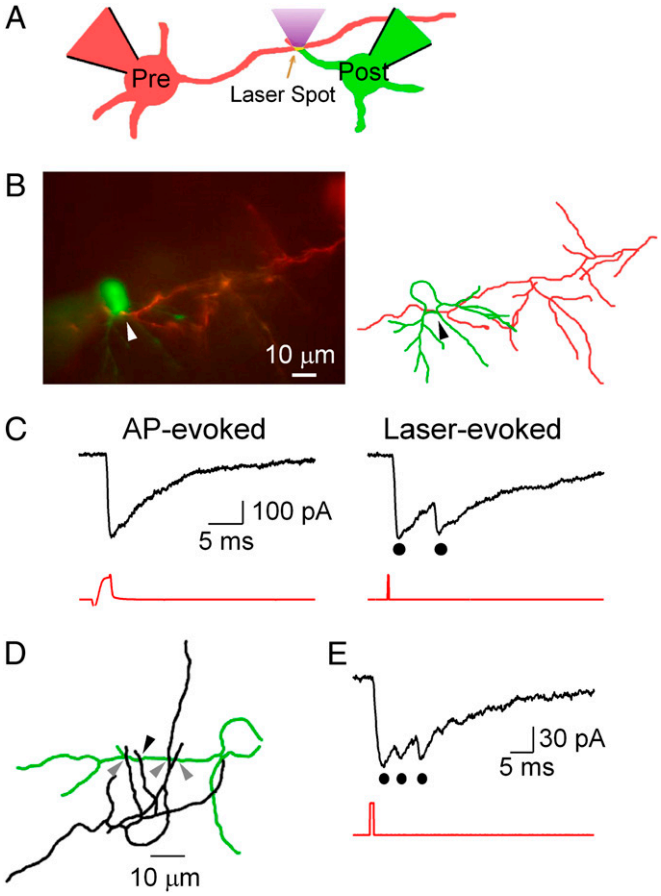

Fig. 1. Neurotransmitter release from single synaptic contacts. (*A*) Schematic of the method used. The presynaptic and postsynaptic cells are filled with red and green Alexa dyes, respectively, to facilitate neurite identification. The presynaptic cell contains DM-nitrophen and OGB-5N. Presynaptic Ca^{2+} uncaging is achieved by delivering a brief, spatially defined laser flash (405 nm) on the synaptic contact. (*B*) Synaptically connected pair (*Left*; Movie S2) and reconstruction (*Right*; red, presynaptic; green, postsynaptic). The arrowhead indicates the contact site for uncaging. (*C*) (*Left*) AP-induced PSC (presynaptic trace in red). (*Right*) Laser-induced PSC doublet (dots). Laser stimulus: duration, 200 μs; energy, 2.9 μJ (red). (*D*) Morphology of an autaptic MLI (somatodendritic compartment is shown in green, and axon is shown in black; Movie S3). Axon collaterals are closely apposed to the dendrites. Potential contacts indicated by gray arrowheads showed no response to photolysis. Contact indicated by the black arrowhead responded to laser stimulation with the PSC shown in *E*. (*E*) Triphasic PSC evoked by laser spot (1 ms, 4.9 μJ) at the location indicated with the black arrowhead in *D*.

expected, whereas the photolysis-induced PSC has two distinct peaks (Fig. 1*C*, black dots) due to a delayed second release. In this example, the main features of the PSC (amplitude, onset, and decay kinetics) are very similar for the spike-induced and laser-induced responses. This indicates that the connection shown in Fig. 1*B* involved a single functional synaptic site, as occurs in a significant proportion of MLI-MLI connections (23).

Single-Site Autaptic Currents. MLIs display autapses, as well as conventional synapses. In autapses, the axon contacts dendrites of the same cell (24) (Fig. 1*D*). Single-site autapses were sometimes found between the axon and the dendrites of a single interneuron, as illustrated (Fig. 1*E*, Fig. S1*C–E*, and Movie S4). Autaptic contacts, like synaptic contacts, displayed a large quantal size, high receptor occupancy, and multiple release events. A comparison between 13 paired and 6 autaptic recordings did not reveal significant differences in peak quantal amplitude (179 ± 138 pA vs. 177 ± 189 pA; $P = 0.97$), 10–90% rise time (1.0 ± 0.8 ms vs. 1.0 ± 0.5 ms; $P = 0.49$), maximum number of released vesicles (2.25 ± 0.7 vs. 2.7 ± 0.8 in a 10-ms period following the laser pulse; $P = 0.5$; laser energies >0.2 μJ), and similar high receptor occupancy indicated by occlusion of postsynaptic receptors (A_2/A_1 ratio: 0.3 ± 0.30 vs. 0.28 ± 0.30; $P = 0.9$) for paired and autaptic synapses, respectively. We conclude that autaptic synapses have properties similar to conventional synapses in MLIs, and the data were pooled for analysis.

Presynaptic Ca^{2+} Changes on Photolysis. The physiological free Ca^{2+} concentration that triggers neurotransmitter release is thought to be localized to the regions around single Ca^{2+} channels (25). With Ca^{2+} uncaging, the aim was to generate a fast, spatially uniform, and sustained increase of free Ca^{2+} concentration with a laser spot of 3 or 5 μm, a little larger than the presynaptic terminal. Two tests demonstrated our ability to target an individual synaptic contact. First, a lateral displacement of a few microns away from the axon always abolished the PSC, and the same result was usually found when displacing the spot from the active site along the axon (Fig. S1 *D* and *E*). In some cases, however, multiple release sites could be identified, corresponding to several contacts with distinct postsynaptic dendrites (Fig. S1 *A* and *B*). Second, the spatial extent of the fluorescence signals due to Ca^{2+} release from DM-nitrophen was sharply constrained to the illumination site (Fig. 2 *A* and *B*). Because sites of presynaptic release from MLI axons are sparse and mostly involve a single active zone (3), these experiments collectively indicate that the laser-induced responses originated in single synaptic sites.

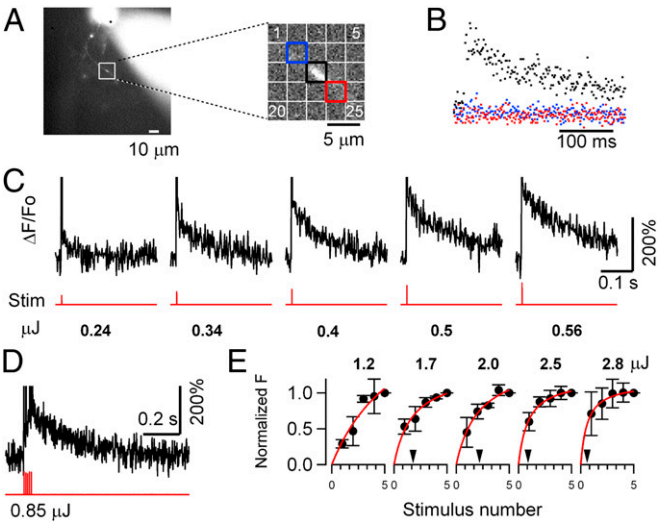

Fig. 2. Laser-evoked calcium transients in MLI axons. (*A*) Localization of photolytic Ca^{2+} release in the axon. (*Left*) Axon morphology shows the location of the recorded site. (*Right*) Detail shows the axon (diagonal: top left to bottom right) and regions of interest (ROIs) used for analysis (laser spot positioned at the center of the square). (*B*) Fluorescence traces from the three ROIs depicted in *A* (same color coding) following Ca^{2+} uncaging by the laser spot in the central ROI. A fluorescence increase was seen only in the central ROI (black trace). (*C*) Fluorescence records ($\Delta F/F_0$) due to Ca^{2+} release by photolysis of DM-nitrophen. Single laser pulses of 0.2-ms duration at energies ranging 0.24–0.56 μJ are indicated by the lower (red) traces. The frame corresponding to the laser flash is neglected. (*D*) Fluorescence response to a train of five laser pulses of 0.1-ms duration at 100 Hz, 0.17 μJ each. (*E*) Summary data show the dependence of $\Delta F/F_0$ on laser intensity and stimulus number (same power scale as in *C*; total energy range: 0.24–2.8 μJ). Fluorescence changes are normalized to the value after the fifth flash. The arrowheads indicate the number of stimuli leading to half saturation (except for the first plot, where this number was just beyond the *x*-axis range).

To determine the time-course and efficiency of DM-nitrophen photolysis in these experiments, we examined the dependence of Ca^{2+} release and consequent ion channel activation on laser intensity. Control photolysis experiments were carried out in MLI somata at −15 mV holding potential with presynaptic internal solution and gave two readings of Ca^{2+} release: a direct one, the fluorescence change in the Ca^{2+} indicator, and an indirect one, the activation of "BK" Ca^{2+}- activated K^+ currents (Fig. S2). Both increased progressively as the laser energy input increased, indicating the range needed to elicit high Ca^{2+} and transmitter release. In the axon, the fluorescence change, $\Delta F/F_0$, due to Ca^{2+} release by laser pulse photolysis (Fig. 2) showed a sharp rise in <1 ms, consistent with rapid Ca^{2+} release by photolysis of DM-nitrophen-Ca^{2+}, which has been reported to have a 15-μs time constant (26). The mean decay time constant of Ca^{2+}-induced fluorescence was 120.7 ± 63.5 ms (mean ± SD; n = 49 regions of interest from 18 different cells; single laser pulses 0.1–1 ms in duration, energies 0.2–5 μJ at the cell). Peak $\Delta F/F_0$ was a sublinear function of laser energy, presumably as the low-affinity Ca^{2+} indicator OGB-5N was progressively saturated (Fig. 2*E* and Fig. S2*B*). These data indicate that the free Ca^{2+} concentration increase due to laser photolysis of DM-nitrophen in the axon is large and prolonged beyond that occurring during normal synaptic release.

Single and Multiple Laser-Induced PSCs at a Single Site. The quantal nature of photolysis-induced synaptic currents at a single release site is illustrated by the sequence of consecutive trials with varied laser energies shown in Fig. 3. When ordered against increasing laser power, the trials successively displayed no response, single responses, and multiple responses exhibiting sublinear amplitude summation (Fig. 3*C*). In this example, latencies decreased from 2 to 4 ms for the single responses to ~0.5 ms at high laser energy (Fig. 3*D*).

In multiple responses, overlapping PSCs have progressively decreasing amplitude changes, as illustrated in Figs. 1 *C* and *E* and 3. These are interpreted as progressive saturation of postsynaptic receptors by successive vesicular release events at single synaptic sites (19, 23, 27). They cannot be explained by dendritic filtering, because the predicted peak current attenuation due to dendritic filtering in MLIs is only 20% at a distance of 50 μm, which is much too weak to explain the observed sublinearity (28). The average distance of synaptic contacts to the center of postsynaptic cells was 18.5 ± 12.7 μm, with a minimum of 2 μm and maximum of 40 μm; we did not observe any correlation between this parameter and receptor occupancy ($P > 0.05$; n = 13; note that the synapses illustrated in Figs. 1*B*, 3*A*, and 4*A* are all within 10 μm of the soma yet display marked sublinear summation). Over all trials, the mean ratio between second and first laser-evoked PSC amplitudes (A_2/A_1 in the scheme of Fig. 3*E*) was 0.23 ± 0.30 (n = 13 cells). This gives a mean postsynaptic receptor occupancy of 77% ($1 - A_2/A_1$) due to a single quantum, which is close to the value given previously for normal transmission at these synapses (76%) (19, 23).

Next, we studied the stochastic variability in quantal release by repeatedly stimulating single synaptic contacts at low frequency with a constant laser energy, as illustrated in Fig. 4. In this case, as in that of Fig. 3, AP-evoked PSCs displayed large and heterogeneous amplitudes [600 ± 200 pA, coefficient of variation (CV) = 0.34], indicating the presence of multiple synaptic contacts between the two neurons (Fig. 4*B*; blue bars in the histogram in Fig. 4*D*). In contrast, laser-evoked PSCs had homogeneous maximum amplitudes (green bars in the histogram in Fig. 4*D*; mean ± SD = 246 ± 14 pA, CV = 0.06) and quantal amplitudes (individual first events in each trace: CV = 0.18). Across experiments, the mean CV for laser-evoked quantal events was 0.21 ± 0.06 (n = 6), similar to CV values previously reported for PSCs originating from a single release site (19, 29, 30). To quantify the number of synaptic contacts made by each presynaptic cell on its postsynaptic partner, we calculated the ratio between the mean amplitude of the PSC induced by a presynaptic AP (excluding failures) and the mean amplitude of the PSC induced by DM-nitrophen photolysis at a single synaptic contact. The average ratio was 1.8 ± 1.3, with a minimum of 0.6 and a maximum of 5.2 (n = 11). Of these pairs, three had a ratio close to 1 (as in Fig. 1*C*), indicating a frequency of 27% single-site connections in our paired recordings similar to that reported previously (31).

In the sequence of responses to a 200-μs laser pulse of high energy shown in Fig. 4*C*, each laser stimulation elicited a burst of quanta released during a period of 10 ms. The number of events in this burst fluctuated across trials, but it remained small in general, and in a given experiment, it appeared to be constrained by an upper limit (three events in the example shown). Over all 14 experiments, the range of the maximum number seen in a single sweep was one to four PSCs per stimulus, with a modal value of 2, as illustrated by the histogram in Fig. 4*E*.

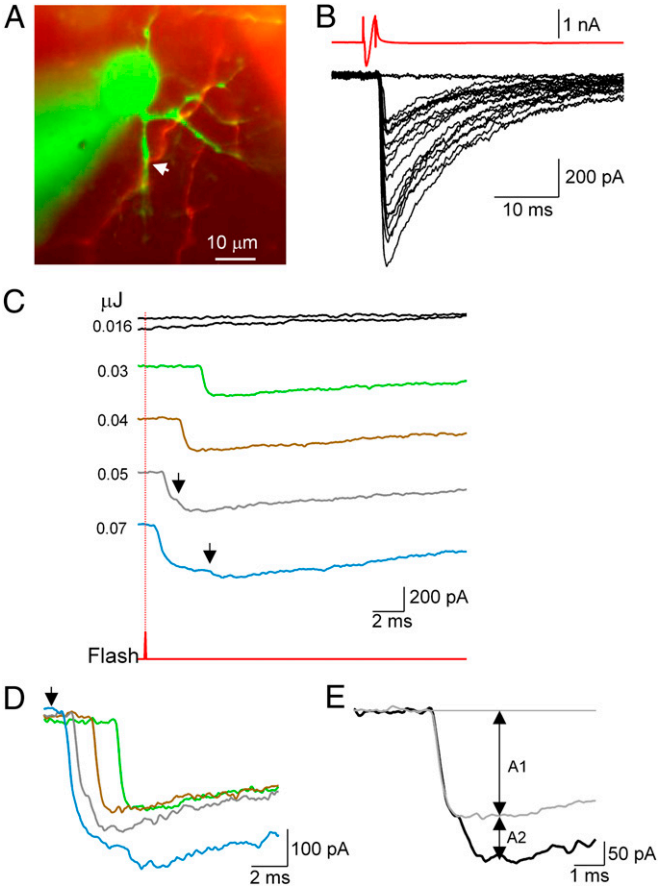

Fig. 3. Superposition of quantal responses at high laser energy. (*A*) Image of synaptically connected presynaptic (red) and postsynaptic (green) MLIs (Movie S5). (*B*) Presynaptic APs elicit large PSCs. (*C*) Laser stimulation at varying energies. Laser timing is indicated by the lower trace (red), and position is shown by the arrow in *A*. Stimulation order: 0.016/0.05/0.03/0.016/0.04/0.07 μJ. Responses are quantal, with variable latencies after the laser pulse. Note the sublinear amplitude summation in multiple responses. (*D*) Superimposition of traces to show latencies; laser timing is indicated by the arrow. The blue trace may represent an unresolved double event (latency of 0.5 ms) followed by a late event (latency of 4.5 ms). (*E*) Analysis of compound PSC (0.05-μJ stimulus, black trace) as a superimposition of quantal responses with amplitude A_1 (light gray trace, average of two single quantal responses) and a delayed quantal response with amplitude A_2. The receptor occupancy by the single quantal response is calculated as $1 - A_2/A_1$, giving 0.58 in the present case.

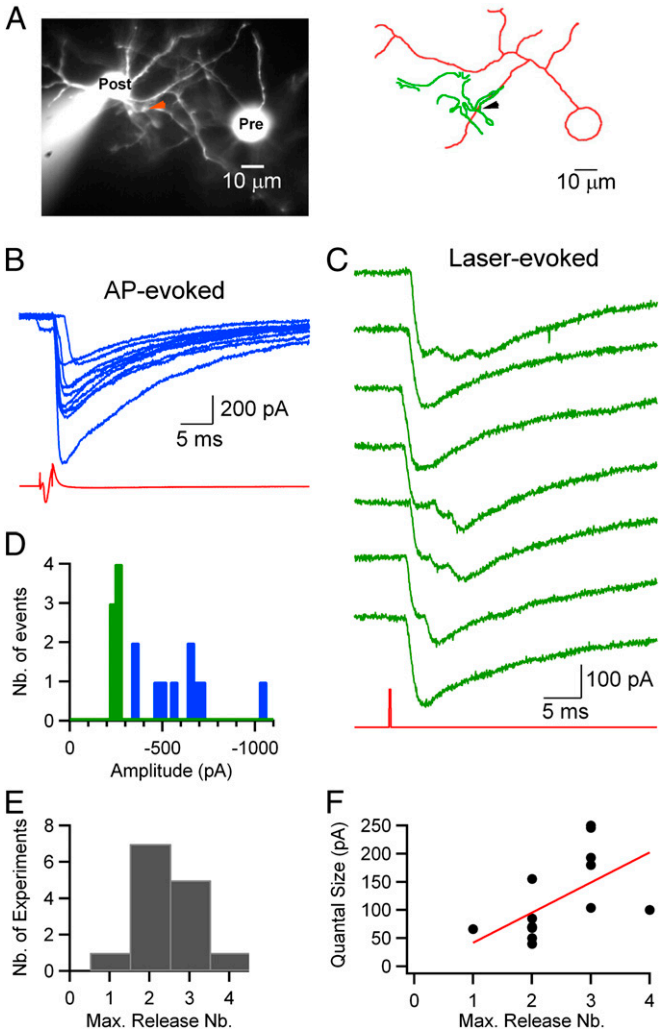

Fig. 4. Number of quanta released by a single stimulation at each synapse. (*A*) Fluorescent image (*Left*) and simplified reconstruction (*Right*; presynaptic soma and axon, red; postsynaptic somatodendritic compartment, green) of a pair of synaptically connected MLIs (Movie S6). The arrowhead shows the uncaging site. (*B*) PSCs (blue records) evoked by presynaptic APs (red trace). (*C*) Laser-evoked PSCs (green) with laser stimulus (red). Laser stimulation: duration, 200 μs; energy, 0.6 μJ; one pulse every 30 s. Estimated number of released vesicles in sequential order: 3/1/2/3/3/2/1. (*D*) Peak amplitude histograms display larger, more variable values for spike-evoked PSCs (blue) than for laser-evoked currents (green), indicating multiple sites of conventional synaptic connection and a single site of laser stimulation. (*E*) Histogram of maximum (Max.) number (Nb.) of release events observed following a single laser stimulus in experiments with repeated stimulations at the same location (laser energies >0.2 μJ, mean maximum value of 2.4 events per site). (*F*) Plot of quantal size as a function of the maximum number of quantal events seen at each site (laser energies >0.2 μJ). The Spearman rank coefficient ($r = 0.7$, $P < 0.02$) indicates correlation between the two parameters. The red line illustrates a linear fit to the data.

Determination of the RRP at a Single Release Site. The duration of the exocytosis burst in Fig. 4*C* is much shorter than that of the presynaptic Ca^{2+} signal measured in axon varicosities (time constant of decay of ~120 ms; Fig. 2). Furthermore, the mean rate of vesicular release observed during the burst is high (250 s^{-1}; see below). Under these conditions, the number of events in the exocytosis burst at a single site represents the number in the RRP (32). The kinetics of quantal release evoked by the high Ca stimulus and the number of events in the exocytosis burst were analyzed in 1-s sweeps following each stimulus.

To obtain a kinetic description of quantal release, the latencies of PSCs were measured from the time of laser stimulation and fitted by maximum likelihood, yielding the probability density functions superimposed on the histograms shown in Fig. 5. Analysis of all experiments (Fig. 5*A*) showed two well-separated exponential components with time constants of 4.0 and 319.6 ms, with 60% of quanta associated with the fast component and 40% associated with the slow component. To examine the rate of release following a Ca^{2+} step, histograms were also made of the latency to the first quantal event. These showed an initial silent

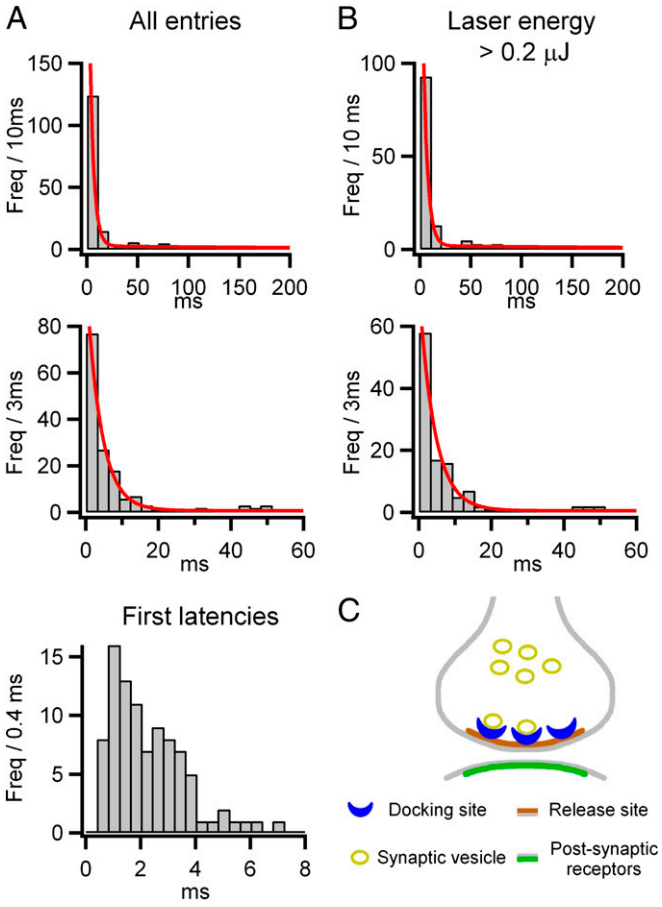

Fig. 5. Latency histograms of release events. (*A*) Histogram of PSC latencies following 86 laser stimulations from 19 single-site recordings (6 autapses and 13 MLI-MLI synapses), measured from the time of the laser pulse (laser energy range: 0.03–5.3 μJ) and displayed at low (*Top*; 10-ms bins; Freq, frequency) and intermediate (*Middle*; 3-ms bins) time resolutions. The intervals were fitted by maximum likelihood with a two-exponential probability density function (red curves superimposed on the histograms) with means of 4.0 ms and 319.6 ms and with areas 60% and 40% of the total. (*Bottom*) Histogram of latencies to the first quantal event shown with high time resolution reveals an initial silent period of 0.4 ms (laser pulse durations ≤0.2 ms). (*B*) Analysis applied to a restricted dataset with high laser energies >0.2 μJ (59 laser stimulations, from 6 autapses and 8 MLI-MLI synapses). The two exponential probability density function time constants are 4.3 ms and 340.0 ms. A total of 61% of the area is associated with the short latency component, corresponding to an average 1.76 ± 0.07 events per stimulus in the fast component. This represents an uncorrected estimate of the RRP size for a single-site synapse. (*C*) Schematic of a small synapse with a single active zone (brown) and associated postsynaptic receptors (green). Synaptic vesicles (yellow) bind to docking sites (blue) before exocytosis. In this view, the RRP is represented by the number of docked vesicles, which varies from stimulus to stimulus, and its value is limited at a given synapse to the total number of available docking sites. Thus, $RRP = N_D * f$ has a mean of $N_D * F$ and maximum N_D, where N_D is the number of docking sites and f is their occupancy at any time, with the mean value F.

period lasting 0.4 ms, followed by a sharp rise to a maximum rate of exocytosis at 1 ms (Fig. 5*A*, *Bottom*). The kinetics likely reflect high cooperativity in the activation by Ca^{2+}, with Ca^{2+}-independent steps late in the exocytosis pathway (15, 16), and they are similar to the stochastic quantal release seen with focal recording at the neuromuscular junction (33).

Analysis of a subset of the data obtained with high laser energies (>0.2 μJ), ensuring strong stimulation, gave similar time constants (4.3 ± 0.4 ms and 339 ± 38 ms) and areas (61 ± 4% and 39 ± 4%) (Fig. 5*B*). To verify that such laser energies were sufficient to empty the RRP, we applied a second stimulus in some experiments, also at high intensity, with a latency of 30–50 ms. The second stimulus failed to elicit any response, confirming total emptying of the RRP by the first stimulus (11 double trials in four experiments; Fig. S3). The mean number of events in the fast component was 1.76 ± 0.07 per laser stimulus. The true number is expected to be higher because some closely spaced events will be missed through postsynaptic receptor saturation, as can be seen in the bursts illustrated in Fig. 4*C*. We calculate that a correction factor of 1.07 needs to be applied for missed events, based on a dead-time of 0.6 ms and using estimates of the event probabilities from first latency histograms (*SI Materials and Methods*). When applied to the observed mean of 1.76, this gives a corrected average of 1.88 events per stimulus associated with the fast component. The fast component represents the initial burst of exocytosis, with a maximum rate of 410 s^{-1} in the first 1–2 ms after the laser pulse. The period of high Ca^{2+} extends into the slow component of exocytosis, where the rate of exocytosis has declined to 1–2 s^{-1} (mean of 1.1 s^{-1}), similar to the rate of spontaneous events (mean of 0.8 ± 0.54 Hz in these experiments). This indicates that Ca^{2+}-dependent replenishment is not fast enough to sustain release and argues against models in which the RRP size depends on vesicle replenishment (34–35). We conclude that our best estimate of the average RRP for a single release site at these synapses is 1.9.

It was noted that the number of quanta associated with each of the bursts shown in Fig. 4*C* varies from sweep to sweep, although the Ca^{2+} stimulus is uniformly strong. This is an unexpected observation, indicating that the RRP estimated in this way may vary from stimulus to stimulus independent of the Ca^{2+} level. We examined more closely the variation in the number of events seen from trial to trial at individual sites stimulated consecutively with high laser energy. In seven experiments with four to seven repetitions at laser energies >0.2 μJ, the mean was 1.78 ± 0.27 events per stimulus and the CV was 0.47 ± 0.18, which is significantly smaller than that predicted from the mean by Poisson statistics (predicted CV = 0.75). Although fluctuations in the number of quanta released were seen ranging between one and four PSCs per stimulus, notably, only a single failure of release was seen. These observations indicate that the RRP does not represent the Poisson condition of a large reservoir of vesicles with small individual release probabilities but, rather, quantal release with high probability from a restricted number of vesicles. If the release is from a fixed number of docking sites at each presynaptic terminal (32), the average fractional occupancy of sites can be estimated as the ratio of the mean number to the maximum number released in each run. This gives the mean occupancy of docking sites as 0.70. Describing release with a simple binomial distribution yields an estimate of 0.41 as the CV, which is close to the observed value of 0.47 (the model is elaborated in *SI Materials and Methods*). Because the waiting time between trials was 1–2 min, which is much longer than the RRP replenishment measured under resting conditions (time constant of 1.7 s) (17), RRP fluctuations presumably reflect spontaneous variations in the occupancy of docking sites rather than incomplete recovery from previous stimulations. Alternatively, it is also possible that the number of docking sites may fluctuate in time. Overall, the data are consistent with a small number of docking sites in each presynaptic terminal, around three, with a high average fractional occupancy of about 0.7 that fluctuates from stimulus to stimulus (as represented by the cartoon in Fig. 5*C*).

In MLIs, the size of synaptic contacts varies widely (from 0.02 to 0.4 $μm^2$, with a mean of 0.152 $μm^2$) and the surface area of the presynaptic active zone is correlated with the number of postsynaptic receptors (3). We have searched for a correlation between the quantal size, as a measure of the size of the synapse, and the number of docking sites recorded at the same synapse. The data are correlated, as shown in Fig. 4*F*, with a Spearman rank coefficient of 0.7 ($P < 0.02$). The correlation of estimated number of docking sites with synaptic size favors an interpretation of multiple vesicle docking sites rather than a single docking site for each synapse.

Discussion

Strategy to Study Single Synaptic Sites. In this report, we describe an approach to study small single synaptic sites in a brain slice preparation, using local photorelease of Ca^{2+} in the presynaptic axon. The resulting presynaptic Ca^{2+} elevation is highly restricted in space. Because the lateral spread of axonal signals (Fig. 2 *A* and *B*) is smaller than intervaricosity distances (mean of 45 ± 21 μm) (36), it is possible to restrict the Ca^{2+} rise to a single presynaptic varicosity. On the postsynaptic side, GABAergic synapses in MLI dendrites have been found to be sparse and compact, thus ensuring that the presynaptically released transmitter reaches a single postsynaptic density (3). Indeed, PSCs display hallmarks (low variability of the peak amplitude and occlusion between events occurring in close succession) that have previously been used to identify signals originating at a single synaptic site (29). Collectively, these results strongly suggest that the present approach successfully provides signals originating from single synaptic sites.

Compared with previous strategies that have been used to obtain single-site signals in MLIs, the present approach offers two key advantages. First, Ca^{2+} uncaging is an accurate and flexible stimulation procedure, which permits repeatedly triggered vesicular release with submillisecond precision. By contrast, in the α-latrotoxin method, where the stochastic action of the toxin at very low concentrations leads to bursts of PSCs originating from single release sites, the strength or duration of the stimulation cannot be easily manipulated (19). Time control is also better than with presynaptic stimulation of simple synapses, where the delays include the unknown propagation times of the AP (31). A second major advantage of the present approach is that the synaptic site is unambiguously identified. This offers the option to modify the ionic or pharmacological environment of the release site selectively in future studies.

At glutamatergic synapses, "optical quantal analysis" has been used to investigate vesicular release at single release sites, using postsynaptic Ca^{2+} signals originating from NMDA receptors (12, 37); however, the resolution is not sufficient to distinguish individual release events in multivesicular responses. In addition, optical quantal analysis, like electrophysiological recording of single synapses, lacks the precise presynaptic Ca^{2+} control provided by Ca^{2+} uncaging.

Comparison of the Present Results with RRP Estimates in Other Preparations. An important goal of this work was to measure the RRP at single synaptic contacts. We obtained an average of 1.9 events per release site and a maximum value across successive trials of one to four release events per site.

Previous estimates of the RRP vary widely, giving rise to contrasted mechanistic interpretations. At hippocampal synapses, estimates of one vesicle per release site have been interpreted as reflecting a single-site, single-vesicle mechanism based either on exocytosis block over the entire active zone following an initial release event ("lateral inhibition") (38) or the supply of one exocytosis site with a small complement of primed vesicles (34). At the other extreme, in cerebellar mossy fiber terminals, a very large estimate (300 per site) was interpreted as a very rapid supply of

vesicles to one exocytosis site from a large reservoir of vesicles (35). Divergences between these earlier studies and the present results may reflect different preparations, possibly glutamatergic vs. GABAergic synapses here, or methodological differences, using trains of APs instead of step calcium stimulation. It is also noted that the present study was performed on juvenile rats (11–17 d of age) and that the RRP may vary with age. On the other hand, our study is consistent with functional results obtained at the calyx of Held with calcium uncaging (32); at the neuromuscular junction with presynaptic AP trains (39); and, notably, with quantitative EM at both preparations (4, 40). In each of these cases, the RRP was interpreted as the number of vesicles bound at specific docking sites, with each synaptic release site having only a few (two to six) docking sites (Fig. 5*C*). Our data, together with these earlier studies, collectively suggest that this may be the building block of many vertebrate synapses.

Materials and Methods

Details of the methods and analysis are given in *SI Materials and Methods*. Briefly, MLIs of cerebellar slices from Sprague–Dawley rats aged 11–17 d were recorded with the whole-cell patch-clamp technique at room temperature. Experimental procedures were approved by the Directorate of Paris Veterinary Services, by the scientific committee of the central animal house of Paris Descartes (Centre Saints Pères) as well as by the ethical committee for animal experimentation of Université Paris Descartes. DM-nitrophen-Ca, Alexa dyes, and the Ca indicator OGB-5N were applied intracellularly by whole-cell recording. Photolysis of DM-nitrophen was with a 1-, 3-, or 5-μm laser spot at 405 nm. Fluorescence excitation was with light-emitting diode light sources, and images were recorded with a CCD camera.

ACKNOWLEDGMENTS. We thank Gordon P. Reid (Medical Research Council, National Institute of Medical Research, United Kingdom) for the synthesis and purification of DM-nitrophen, Remigijus Lape (University College London) for data conversion to the DCProgs format, Christophe Pouzat for an estimate of the proportion of missed events using simulations of the model in Fig. 5C, and Philippe Ascher, Céline Auger, Isabel Llano, and Brandon Stell for critical comments on the manuscript. This work was supported by the Fondation pour la Recherche Médicale (A.M.), Contract BLAN08-2_31083 of the Agence Nationale de la Recherche (to A.M. and D.O.), European Union Strep "Photolysis" Grant LSHM-CT-2007-037765 (to D.O.), the Japan Society for the Promotion of Science (KAKENHI Nr.24300144, 24650218, and Core-to-Core Program, all to T.S.), the Toray Science Foundation (T.S.), and the Uehara Foundation (T.S.).

1. Fatt P, Katz B (1952) Spontaneous subthreshold activity at motor nerve endings. *J Physiol* 117(1):109–128.
2. Del Castillo J, Katz B (1954) Quantal components of the end-plate potential. *J Physiol* 124(3):560–573.
3. Nusser Z, Cull-Candy S, Farrant M (1997) Differences in synaptic GABA(A) receptor number underlie variation in GABA mini amplitude. *Neuron* 19(3):697–709.
4. Sätzler K, et al. (2002) Three-dimensional reconstruction of a calyx of Held and its postsynaptic principal neuron in the medial nucleus of the trapezoid body. *J Neurosci* 22(24):10567–10579.
5. Micheva KD, Busse B, Weiler NC, O'Rourke N, Smith SJ (2010) Single-synapse analysis of a diverse synapse population: Proteomic imaging methods and markers. *Neuron* 68 (4):639–653.
6. Ryan TA, Reuter H, Smith SJ (1997) Optical detection of a quantal presynaptic membrane turnover. *Nature* 388(6641):478–482.
7. Nauen DW (2011) Methods of measuring activity at individual synapses: A review of techniques and the findings they have made possible. *J Neurosci Methods* 194(2): 195–205.
8. Schweizer FE, Ryan TA (2006) The synaptic vesicle: Cycle of exocytosis and endocytosis. *Curr Opin Neurobiol* 16(3):298–304.
9. Neher E (2010) What is rate-limiting during sustained synaptic activity: Vesicle supply or the availability of release sites. *Front Synaptic Neurosci* 2:144.
10. Zucker RS, Regehr WG (2002) Short-term synaptic plasticity. *Annu Rev Physiol* 64: 355–405.
11. Miesenböck G, De Angelis DA, Rothman JE (1998) Visualizing secretion and synaptic transmission with pH-sensitive green fluorescent proteins. *Nature* 394(6689):192–195.
12. Yuste R, Majewska A, Cash SS, Denk W (1999) Mechanisms of calcium influx into hippocampal spines: Heterogeneity among spines, coincidence detection by NMDA receptors, and optical quantal analysis. *J Neurosci* 19(6):1976–1987.
13. Berglund K, Kuner T, Feng G, Augustine GJ (2011) Imaging synaptic inhibition with the genetically encoded chloride indicator Clomeleon. *Cold Spring Harb Protoc* 2011 (12):1492–1497.
14. Delaney KR, Zucker RS (1990) Calcium released by photolysis of DM-nitrophen stimulates transmitter release at squid giant synapse. *J Physiol* 426:473–498.
15. Schneggenburger R, Neher E (2000) Intracellular calcium dependence of transmitter release rates at a fast central synapse. *Nature* 406(6798):889–893.
16. Bollmann JH, Sakmann B, Borst JG (2000) Calcium sensitivity of glutamate release in a calyx-type terminal. *Science* 289(5481):953–957.
17. Sakaba T (2008) Two $Ca^{(2+)}$-dependent steps controlling synaptic vesicle fusion and replenishment at the cerebellar basket cell terminal. *Neuron* 57(3):406–419.
18. Burgalossi A, et al. (2010) SNARE protein recycling by αSNAP and βSNAP supports synaptic vesicle priming. *Neuron* 68(3):473–487.
19. Auger C, Marty A (1997) Heterogeneity of functional synaptic parameters among single release sites. *Neuron* 19(1):139–150.
20. Llano I, Gerschenfeld HM (1993) Inhibitory synaptic currents in stellate cells of rat cerebellar slices. *J Physiol* 468:177–200.
21. Kaplan JH, Ellis-Davies GC (1988) Photolabile chelators for the rapid photorelease of divalent cations. *Proc Natl Acad Sci USA* 85(17):6571–6575.
22. Trigo FF, Corrie JET, Ogden D (2009) Laser photolysis of caged compounds at 405 nm: Photochemical advantages, localisation, phototoxicity and methods for calibration. *J Neurosci Methods* 180(1):9–21.
23. Auger C, Kondo S, Marty A (1998) Multivesicular release at single functional synaptic sites in cerebellar stellate and basket cells. *J Neurosci* 18(12):4532–4547.
24. Pouzat C, Marty A (1998) Autaptic inhibitory currents recorded from interneurones in rat cerebellar slices. *J Physiol* 509(Pt 3):777–783.
25. Simon SM, Llinás RR (1985) Compartmentalization of the submembrane calcium activity during calcium influx and its significance in transmitter release. *Biophys J* 48(3): 485–498.
26. Faas GC, Karacs K, Vergara JL, Mody I (2005) Kinetic properties of DM-nitrophen binding to calcium and magnesium. *Biophys J* 88(6):4421–4433.
27. Tang CM, Margulis M, Shi QY, Fielding A (1994) Saturation of postsynaptic glutamate receptors after quantal release of transmitter. *Neuron* 13(6):1385–1393.
28. Pouzat C, Marty A (1999) Somatic recording of GABAergic autoreceptor current in cerebellar stellate and basket cells. *J Neurosci* 19(5):1675–1690.
29. Auger C, Marty A (2000) Quantal currents at single-site central synapses. *J Physiol* 526 (Pt 1):3–11.
30. Kraushaar U, Jonas P (2000) Efficacy and stability of quantal GABA release at a hippocampal interneuron-principal neuron synapse. *J Neurosci* 20(15):5594–5607.
31. Kondo S, Marty A (1998) Synaptic currents at individual connections among stellate cells in rat cerebellar slices. *J Physiol* 509(Pt 1):221–232.
32. Neher E, Sakaba T (2008) Multiple roles of calcium ions in the regulation of neurotransmitter release. *Neuron* 59(6):861–872.
33. Katz B, Miledi R (1965) The effect of temperature on the synaptic delay at the neuromuscular junction. *J Physiol* 181(3):656–670.
34. Hanse E, Gustafsson B (2001) Vesicle release probability and pre-primed pool at glutamatergic synapses in area CA1 of the rat neonatal hippocampus. *J Physiol* 531 (Pt 2):481–493.
35. Saviane C, Silver RA (2006) Fast vesicle reloading and a large pool sustain high bandwidth transmission at a central synapse. *Nature* 439(7079):983–987.
36. Forti L, Pouzat C, Llano I (2000) Action potential-evoked Ca^{2+} signals and calcium channels in axons of developing rat cerebellar interneurones. *J Physiol* 527(Pt 1): 33–48.
37. Oertner TG, Sabatini BL, Nimchinsky EA, Svoboda K (2002) Facilitation at single synapses probed with optical quantal analysis. *Nat Neurosci* 5(7):657–664.
38. Stevens CF, Wang Y (1995) Facilitation and depression at single central synapses. *Neuron* 14(4):795–802.
39. Ruiz R, et al. (2011) Active zones and the readily releasable pool of synaptic vesicles at the neuromuscular junction of the mouse. *J Neurosci* 31(6):2000–2008.
40. Nagwaney S, et al. (2009) Macromolecular connections of active zone material to docked synaptic vesicles and presynaptic membrane at neuromuscular junctions of mouse. *J Comp Neurol* 513(5):457–468.